Chemical Engineering Journal 389 (2020) 124435

Contents lists available at ScienceDirect

Chemical Engineering Journal

journal homepage: www.elsevier.com/locate/cej

Self-alignment of cationic graphene oxide nanosheets for anticorrosive reinforcement of epoxy coatings

Xiaobo Zhu, Qingqing Yan, Li Cheng, Hao Wu, Haichao Zhao*, Liping Wang*

Key Laboratory of Marine Materials and Related Technologies, Zhejiang Key Laboratory of Marine Materials and Protective Technologies, Ningbo Institute of Materials Technology and Engineering, Chinese Academy of Sciences, Ningbo 315201, China

HIGHLIGHTS

- A novel cationic dopamine-reduced graphene oxide ($DRGO^+$) nanosheet was prepared.
- The cationic $DRGO^+$ nanosheets can be self-aligned parallel arrangement in the coating.
- The highly parallel $DRGO^+$ greatly enhances the physical barrier effect of the coating.
- The composite coating has extraordinary anti-corrosion.

GRAPHICAL ABSTRACT

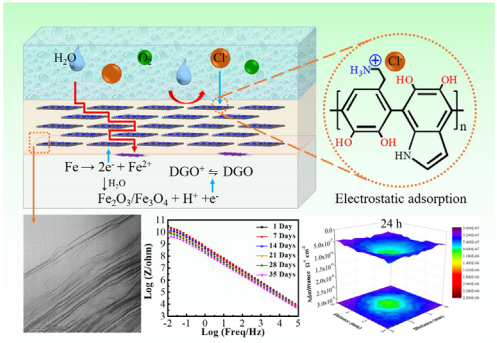

ARTICLE INFO

Keywords:
Graphene oxide
Dopamine
Self-alignment
Electrophoresis
Anti-corrosion

ABSTRACT

Designing coatings with long term anticorrosion performance remains a great challenge. Herein, a newfangled cationic dopamine-reduced graphene oxide ($DRGO^+$) nanosheet is prepared as a filler for epoxy coating via simple dopamine oxidative self-polymerization and ionization reaction. $DRGO^+$ can be dispersed stably in commercial water-based cathodic epoxy emulsion for more than 45 days without precipitation. Due to the presence of $-NH_3^+$ in $DRGO^+$, it can be self-aligned parallel arrangement in the composite coating ($DRGO^+$/EP coating) under the electric field. This highly parallel $DRGO^+$ nanosheets tremendously improve the physical barrier effect of the coating and prolong the penetration path of the corrosive medium. Electrochemical impedance spectroscopy (EIS) test showed that the initial low-frequency impedance modulus of 0.5%-$DRGO^+$/EP coating is as high as $4.79 \times 10^{10}\ \Omega\ cm^2$ when the content of $DRGO^+$ is 0.5 wt%, which is an order of magnitude higher than that of pure epoxy coating ($4.07 \times 10^9\ \Omega\ cm^2$), exhibiting extraordinary corrosion resistance. Finally, the protective mechanism of composite coating is revealed by the identification of corrosion products and local-EIS techniques. In view of the validity of $DRGO^+$, this work highlights the potential route for the large-scale preparation of coatings with superior long-term anti-corrosion.

1. Introduction

With the rapid development of the marine industry and its strong demand for marine resources, various marine facilities, ships and metal components are facing severe marine environmental corrosion issues [1–4]. So far, in addition to reasonable selection of materials, effective

* Corresponding authors.
E-mail addresses: zhaohaichao@nimte.ac.cn (H. Zhao), wangliping@nimte.ac.cn (L. Wang).

https://doi.org/10.1016/j.cej.2020.124435
Received 30 October 2019; Received in revised form 6 January 2020; Accepted 12 February 2020
Available online 19 February 2020

measures to prevent and mitigate marine corrosion rely on coating technology and surface treatment [5,6]. Among them, organic coatings, such as epoxy resin, acrylic resin, and polyurethane, are widely used in metal anticorrosion owing to their good physical barriers [7–9]. In particular, water-based cathodic epoxy electrophoretic emulsions are not only green and environmentally friendly (meet the requirements of low volatile organic compounds emissions), but also has desirable adhesion and extensively employed in mainstream automobile and ship coatings [2,10]. However, organic coatings have a certain permeability to H_2O, O_2 and Cl^- in corrosive media [11,12]. Accordingly, a great deal of work has focused on improving the impermeability of organic coatings to enhance their corrosion resistance [13–16].

Layered nano-fillers (i.e., clay, boron nitride, graphene, and so forth), with high aspect ratio and good ability to restrain corrosive substances' penetration and diffusion, can effectively address aforementioned issues [17–19]. Pinnavaia et al. reported the greatly reduced the oxygen permeability of the composite coating by adding montmorillonite clay to the epoxy resin [20]. Husain et al. mixed boron nitride with polymer to form hybrid coating, and further improved the corrosion resistance of the composites coating by virtue of the hydrophobic, inert and dielectric properties of boron nitride [21]. Qiu et al. prepared graphene-epoxy resin composites coating on steel surface, showing that the addition of graphene can effectively enhance the anticorrosion of the coating [7]. Nevertheless, because of the van der Waals force between the layered nano-fillers, it is easy to aggregate in the polymer matrix [16], so the preparation of well-dispersed nano-fillers is the key to improve the anti-corrosion of the composite coatings.

Graphene oxide (GO), a momentous ramification of graphene, is more easily functionalized covalently and/or noncovalently owing to the presence of functional groups such as hydroxyl, carboxyl, and epoxy groups, leading to improved compatibility between the GO and solvents/polymers [22–24]. In addition, GO has a high aspect ratio, a high specific surface, and an outstanding ability to block the penetration of corrosive substances, so it is easy to be applied in the anti-corrosion field. Zhang et al. prepared a GO-based sulfonated oligoaniline coating by combining 3-aminobenzenesulfonic acid with oligoaniline on the surface of carbon steel. With the synergistic effect of GO and SAT, the diffusion path of corrosive media in the coating was longer and more tortuous, so as to improve the corrosion resistance of the composite coating [25]. Ramezanzadeh et al. improved the ionic resistance and barrier properties of epoxy coatings by using polyaniline to functionalize the graphene oxide amino group, thereby improving the corrosion resistance of the composite coating [26]. In addition, Lu et al. calculated that the nanosheets with high aspect ratio and in-plane alignment can further improve the barrier properties perpendicular to the alignment direction [27]. Li et al. investigated the effect of 3D random distribution of graphene and in-plane arrangement of graphene on the corrosion performance of the coating, the results showed that the parallel arrangement of graphene in coating has better physical barrier effect and corrosion resistance [13]. Inspired by their work, the preparation of nanosheets with good dispersibility and parallel arrangement in the coating can significantly improve the barrier properties and corrosion resistance of the coating. Notably, electrophoretic deposition technique can enables the charged nanosheets in the electrolyte to be move towards the metal substrate under the electric field forces and deposit in parallel to the surface of the substrate. Therefore, obtaining charged GO nanosheets that can be stably dispersed in a water-based epoxy emulsion is the key to this study.

Dopamine (DA) is rich in catechol and amine groups, which can be used as the active site for covalent modification with the required molecules [28]. Hence, in this work, we prepared a novel cationic dopamine-reduced graphene oxide ($DRGO^+$) nanosheet by a simple oxidative self-polymerization and ionization reaction. Due to the presence of $–NH_3^+$ in $DRGO^+$, it can be dispersed stably in commercial water-based cathodic epoxy emulsion. In addition, under the action of electric field, $DRGO^+$ is moved to the surface of the cathode (Q235 carbon steel) by electrophoretic deposition technology to form composite coating, and then the distribution of RGO in the composite coating with different $DRGO^+$ contents and its influence on the corrosion performance are compared. Finally, local electrochemical impedance spectroscopy (LEIS) techniques, electrochemical impedance spectroscopy (EIS) test, salt spray experiments and corrosion products analysis are used to reveal the corrosion mechanism of the coating. The corrosion resistance of the composites coating is significantly improved attribute to the close self-aligned parallel arrangement of $DRGO^+$ nanosheets in the epoxy coating.

2. Experimental section

2.1. Materials

GO was supplied by Suzhou Carbon Graphene Technology Co., Ltd. Water-based Cathodic epoxy resin electrophoresis emulsion (solid content: 35%) was purchased from Jiangxi Gaojie Technology Co., Ltd. Tris-buffer, dopamine hydrochloride (98% pure), ethanol, acetone (AR), and acetic acid (99.9% pure) were purchased from Aladdin Industrial Corporation without further treatment. Corrosion studies were carried out using Q235 carbon steel substrate ($3 \times 3 \times 0.2$ cm^3).

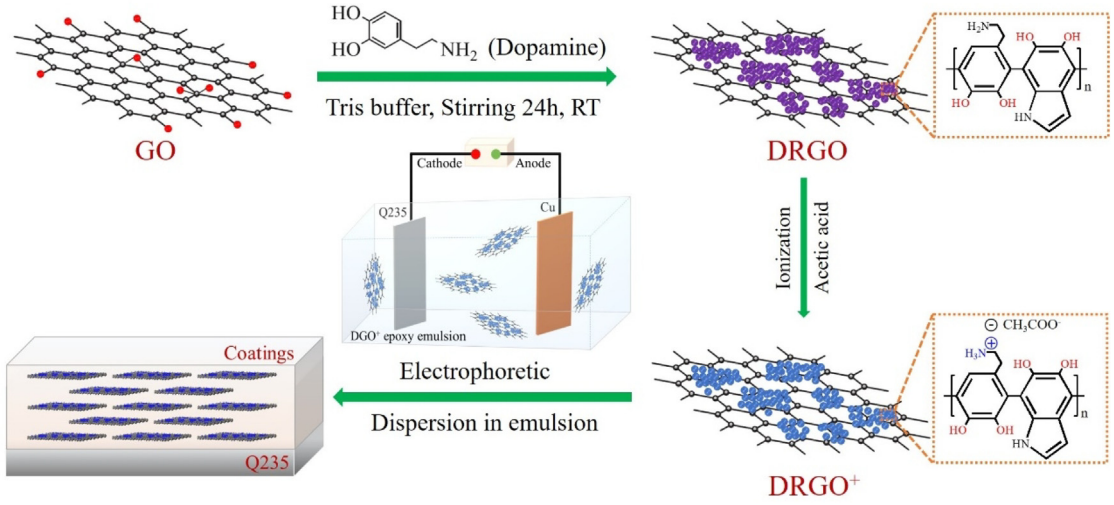

Fig. 1. Schematic diagram of cationic dopamine-reduced graphene oxide ($DRGO^+$) synthesis and electrophoretic deposition process.

2.2. Synthesis of DRGO$^+$

DRGO$^+$ was synthesized via a simple dopamine oxidative self-polymerization and ionization reaction (Fig. 1). Specifically, 0.5 g of GO was added to 250 mL of Tris-buffer solution (10 mM, PH = 8.5) and ultrasonically dispersed for 30 min at 100 KHz. Then 1.5 g of dopamine hydrochloride was added to the above suspension and stirred at ambient temperature for 24 h. The resulting mixture was centrifuged, washed three times with water and ethanol, and dried in a vacuum oven at 40 °C for 24 h to obtain dopamine-reduced graphene oxide (DRGO). Finally, DRGO$^+$ is obtained by ionization of DRGO. Typically, 1 g of DRGO was added to 40 mL of acetone and sonicated for 30 min. Then 2.7 g of acetic acid was slowly added into the above solution and stirred at 28 °C for 3 h. The obtained mixture was centrifuged and dried, and then dispersed in deionized water for further use.

2.3. Preparation of electrophoresis emulsion

The 10.0 g of DRGO$^+$ aqueous dispersion (0.5 g of DRGO$^+$) was slowly added into the 90.0 g of cathodic epoxy resin electrophoresis emulsion containing 15% solid content. After vigorous stirring for 30 min, it was dispersed by ultrasound for 2 h to produce gray dispersion without precipitation. The mixed emulsion is very stable, and has no obvious precipitation after standing for 45 days (as shown in Supporting Information Fig. S1). For the convenience of comparison, mixed emulsions with different DRGO$^+$ contents (0 wt%, 0.25 wt%, and 1.0 wt%) were prepared by the same method.

2.4. Fabrication of coatings

In this study, Q235 low carbon steel was used as the substrate for the epoxy coating. Prior to electrophoretic deposition, all Q235 surfaces were sequentially polished using 400, 800, and 1500 C sandpaper, then ultrasonically washed in ethanol and blown dry with nitrogen. The mixed emulsion was placed in a 200 mL beaker and pretreated copper and steel were used as the anode and cathode, respectively. The coating was deposited by electrophoresis at 60 V and room temperature for 5 min. The coated sample is then washed several times with deionized water to remove residual emulsion from the surface. Finally, the coated sample was dried at 150 °C for 20 min to obtain epoxy composite coating. For convenience, the coatings obtained by emulsion deposition with different DRGO$^+$ contents were labeled as pure-EP, 0.25%-DRGO$^+$/EP, 0.5%-DRGO$^+$/EP, and 1.0%-DRGO$^+$/EP, respectively.

2.5. Characterization

The Fourier transform infrared (FTIR) spectra of GO and synthesized samples were collected on the FTIR spectrometer (Nicolet 6700), and the wavenumber range was 500–4000 cm^{-1}. The Renishaw Invia spectrometer (Renishaw, England) and XPS (Axis Ultra DLD, Kratos, England) were used to obtain the composition and structure of samples. Thermogravimetric analysis was carried out using a Q500 thermogravimetric analyzer (TA Instruments) under an argon atmosphere (200 mL/min) at a heating rate of 10 °C min^{-1}. The morphology and thickness of samples were measured using scanning probe microscopy (SPM, Dimension 3100). The morphology and structure of samples and coatings were tested by S4800 (Hitachi) and FEI Quanta FEG 250 (FEI) scanning electron microscope. The microstructures were further characterized by using high-resolution transmission electron microscope (HRTEM) (Talos F200x). XRD measurements were presented on D8 Advance Davinci (Bruker AXS), where Cu-K$_\alpha$ radiation $\lambda = 1.54178$ Å, ranging from $10^\circ \le 2\theta \le 90^\circ$.

2.6. Corrosion test of coatings

The corrosion performance of the coatings were tested by EIS test, salt spray experiments, and LEIS techniques. The open circuit potential (OCP) and EIS tests of different coatings at different immersion times were evaluated on a CHI-660E electrochemical workstation (China). The electrochemical workstation adopts the conventional three-electrode system, in which the coatings serves as the working electrode (exposed area is 1 cm^2), the saturated calomel serves as the reference electrode, and the platinum slice of 2.5 cm^2 serves as the counter electrode. The EIS tests were conducted in a frequency range of 10^5–10^{-2} Hz with an amplitude of 20 mV. Finally, ZSimpWin software was used to fit the recorded data. Furthermore, the microstructure and composition of the corrosion products on the coatings surface were identified by SEM (FEI Quanta FEG 250) and XRD. The salt spray and LEIS tests were used to present the corrosion speed and corrosion degree of the artificial scratch on the coating. The salt spray test was carried out by spraying 3.5 wt% NaCl solution (pH = 7) according to ISO 3768-1976 and GB 6458-86 standards. LEIS measurements were collected on a VersaSCAN micro-area electrochemical scanning system. Artificial scratches on the surface of the coating was introduced through the scalpel. The admittance mapping of the coatings were recorded with a frequency of 1000 Hz over a region of 3 × 3 mm^2.

3. Results and discussion

3.1. Structure characterizations of DRGO$^+$

The schematic diagram of DRGO$^+$ nanosheet synthesis process is shown in Fig. 1. Firstly, dopamine adheres to the GO surface by oxidation self-polymerization to obtain DRGO. Secondly, DRGO$^+$ with positive charge is obtained by ionizing DRGO with acetic acid. The zeta potential of GO and DRGO$^+$ are measured by a Zetasizer Nano ZS (Fig. S2), the results showed that the potentials of the GO in water dispersion (0.5 mg/mL) and DRGO$^+$ in water dispersion (0.5 mg/mL) are −21.1 mV and +26.3 mV, respectively. In addition, the chemical bond changes of samples can be confirmed by FTIR spectroscopy (Fig. 2a). Obviously, GO mainly contains five absorption peaks, located at 1055, 1211, 1614, 1725, and 3402 cm^{-1}, corresponding to the stretching vibration of C–O bond in epoxy group, C–OH bond, C=C bond in benzene ring, C=O in carboxyl group, and O–H bond, respectively [29,30]. After DA modification, new absorption peaks appeared at 1394 and 1504 cm^{-1} in the FTIR spectrum of DRGO, belonging to C–N structural vibration and N–H tensile vibration respectively, indicating that DRGO was successfully synthesized [24,31]. Moreover, it can be seen from the infrared spectrum of DRGO$^+$ that the N–H peak at 1504 cm^{-1} disappears and a new absorption peak appears near 1173 cm^{-1}, which also corresponds to the stretching vibration of N–H, indicating the successful preparation of DRGO$^+$.

The Raman spectrum of the samples are shown in Fig. 2(b). All three samples have typical D and G peaks near 1345 and 1600 cm^{-1} [32]. The Gaussian fitting calculations showed that the I_D/I_G ratios (area ratio of D peak to G peak) of GO, DRGO, and DRGO$^+$ samples are 1.12, 1.14, and 1.15, respectively [33], and the ratio of I_{2D}/I_G are 2.24, 2.11, and 2.06, respectively. It shows that DA modified and ionized DRGO did not introduce any defects and retained the basic structural characteristics of GO [34]. The elemental composition and chemical bond changes of the three samples can be reflected from the XPS spectrum (Fig. 2c). The XPS full spectrum of GO mainly includes the C 1s peak at 284.5 eV and the O 1s at 531.0 eV, while the N 1s near 397.9 eV appear in the XPS full spectrum of DRGO and DRGO$^+$. In addition, there are four peaks in the C 1s fine spectrum of GO (Fig. 2d), including C–C (284.3 eV), C–O (286.7 eV), C=O (287.3 eV), and O–C=O (288.9 eV) [35]. However, there are five peaks in the C1s fine spectrum of DRGO and DRGO$^+$ (Fig. 2e and f), including C–C (284.3 eV), C-N (285.5 eV), C–O (286.7 eV), C=O (287.3 eV), and O–C=O (288.9 eV) [36]. A new C–N peak appears, and the peaks areas of C–O and C=O in the fine spectrum of C 1s of DRGO and DRGO$^+$ are decreased. The N 1s fine spectrum in DRGO mainly includes C–N at 398.1 eV and HN–C=O at 399.9 eV

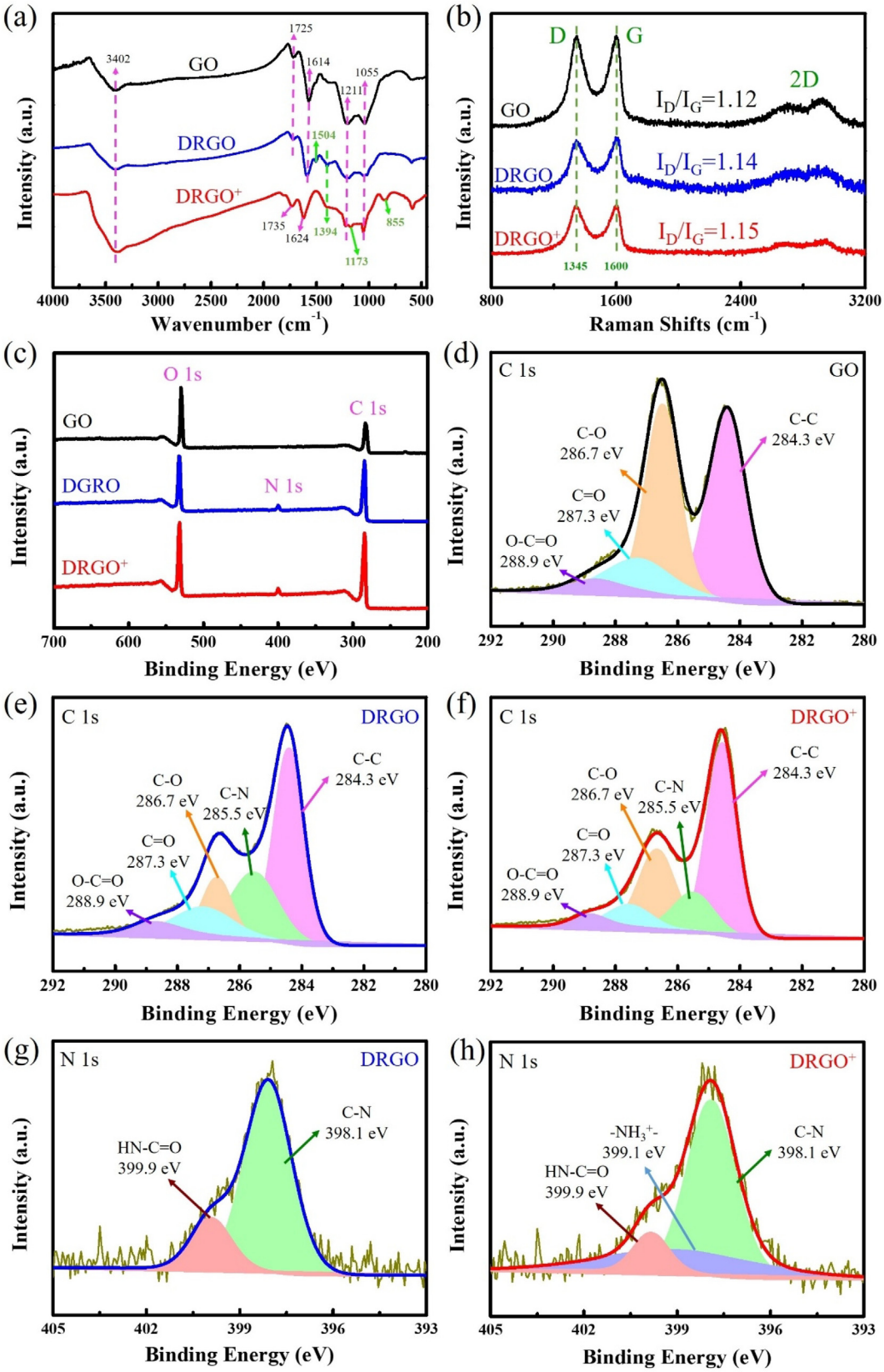

Fig. 2. (a) FT-IR, (b) Raman, and (c) XPS full spectra of GO, DRGO, and DRGO$^+$; XPS C 1s fine spectra of (d) GO, (e) DRGO, and (f) DRGO$^+$; and XPS N 1s fine spectra of (g) DRGO and (h) DRGO$^+$.

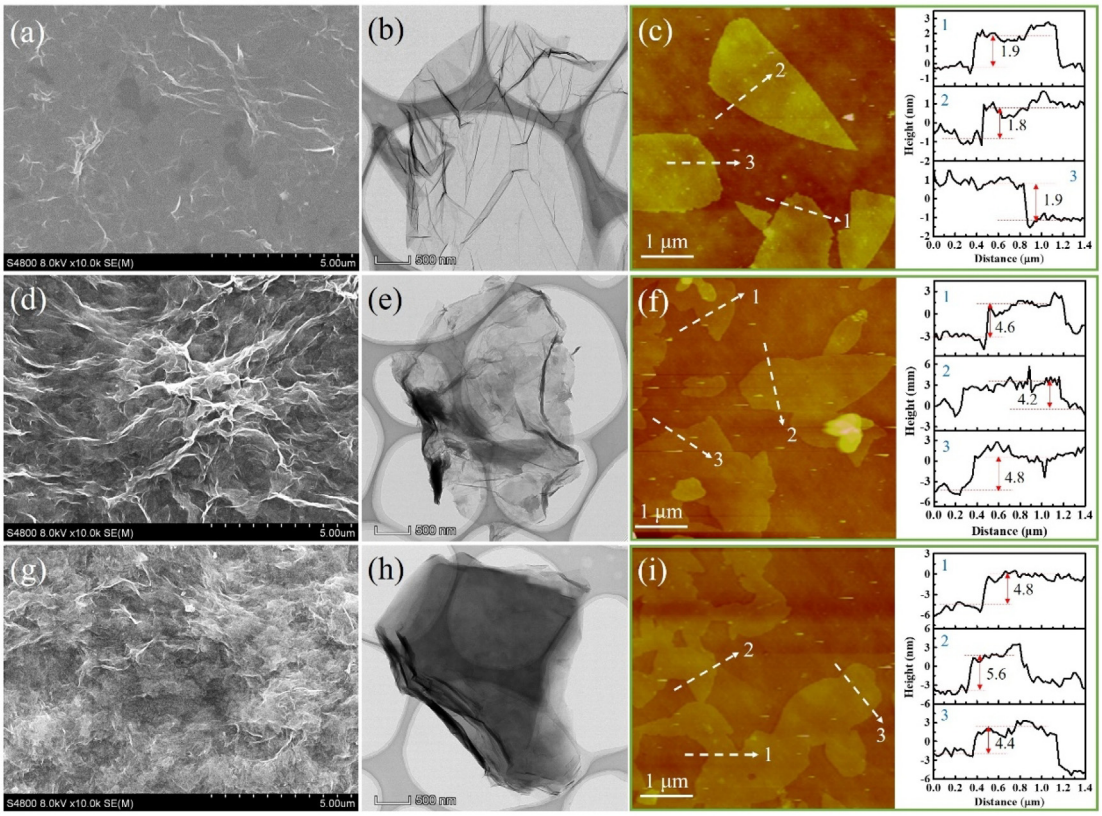

Fig. 3. SEM, TEM, and SPM images of (a–c) GO, (d–f) DRGO, and (g–i) DRGO$^+$ after dispersion in ethanol, respectively.

(Fig. 2g), while the N 1s fine spectrum in DRGO$^+$ has a new amino group (–NH_3^+–) of 399.1 eV (Fig. 2h) [2]. Therefore, we can confirm that DRGO is ionized by acetic acid to form DRGO$^+$. The existence of these bonds also indicates the successful synthesis of DRGO and DRGO$^+$. This is consistent with the conclusions obtained from the FTIR spectrum.

3.2. Morphology of DRGO$^+$

The surface topography and morphological changes of GO, DRGO and DRGO$^+$ are observed by SEM, TEM and SPM, as shown in Fig. 3. It can be seen from the SEM (Fig. 3a) and TEM (Fig. 3b) images of GO that GO is smooth, transparent and thin. In contrast, the surface of DRGO is more uneven, curly and less transparent (Fig. 3d and e), and there are obvious particles on the surface, which is attributed to the introduction of DA. On the other hand, the surface of DRGO$^+$ is also uneven, curled, and has lower transparency (Fig. 3g and h). The microstructure is not changed much compared with DRGO, except that the surface black particles become uniform. Furthermore, the addition of DA and ionization hardly affected the structure of GO, which is consistent with the Raman analysis. SPM further examined the surface topography and thickness of GO, DRGO, and DRGO$^+$. Clearly, GO, DRGO, and DRGO$^+$ all exhibit a sheet-like structure. The thickness of GO is about 1.9 nm, and the thickness of DRGO and DRGO$^+$ are not much different, approximately 4.6 nm and 4.8 nm, respectively, which is increased compared with GO, indicating that DA is successfully grafted on the GO surface.

3.3. Morphology and structure of coatings

The surface and cross-sectional SEM images of pure-EP, 0.25%-DRGO$^+$/EP, 0.5%-DRGO$^+$/EP, and 1.0%-DRGO$^+$/EP coatings are shown in Fig. 4(a, e, i, and m) and Fig. 4(b, f, j, and n), respectively. Obviously, with the increase of DRGO$^+$ content, the roughness of the coating surface first decreased and then increased, indicating that the DRGO$^+$ nanosheets is successfully deposited in the coating during the electrophoretic deposition. In addition, cross-sectional SEM images of the coating showed that the thickness of the four coatings deposited under the same conditions is about 25.2 μm. And as the content of DRGO$^+$ increases, the cross-sectional of the coating becomes smoother. This is attributed to the fact that during the electrophoretic deposition process, the molecular brush of the positively charged DRGO$^+$ surface will accelerate the movement of the emulsion towards the cathode, resulting the coating denser and smoother. The TEM samples of the coatings are obtained by taking coatings cross-sectional with a focused ion beam (FIB) apparatus. The TEM images of the pure-EP coating are shown in Fig. 4(c and d), and it can be seen that the interior of the pure-EP coating only exhibits epoxy matrix. From the TEM images of the 0.25%-DRGO$^+$/EP coating (Fig. 4g and h), it can be seen that in the interior of the coating, in addition to the epoxy matrix, a layered arrangement RGO appeared, which is more pronounced in the HRTEM. It indicates that DRGO$^+$ nanosheets can be self-aligned and parallel arranged in the coating under the action of electric field, which is beneficial to improve the physical barrier effect and corrosion resistance of coating. With the increase of DRGO$^+$ content, the layered arrangement RGO in TEM images becomes more and more obvious and longer, as shown in Fig. 4(k) and (l). However, when the DRGO$^+$ content increased to 1.0 wt%, small bright voids appeared in the TEM images of the coating (Fig. 4o and p), which may be the pores generated by the distribution of graphene in the coating. This will degrade the corrosion performance of the coating. In this study, the main driving force of self-alignment is electric field force. The DRGO$^+$ nanosheets uniformly dispersed in the water-based cathodic epoxy emulsion can move rapidly toward the cathode under the action of electric field. At the same time, during the electrodeposition process, DRGO$^+$ nanosheets also undergo self-aligned alignment in the plane in the epoxy. In addition, the

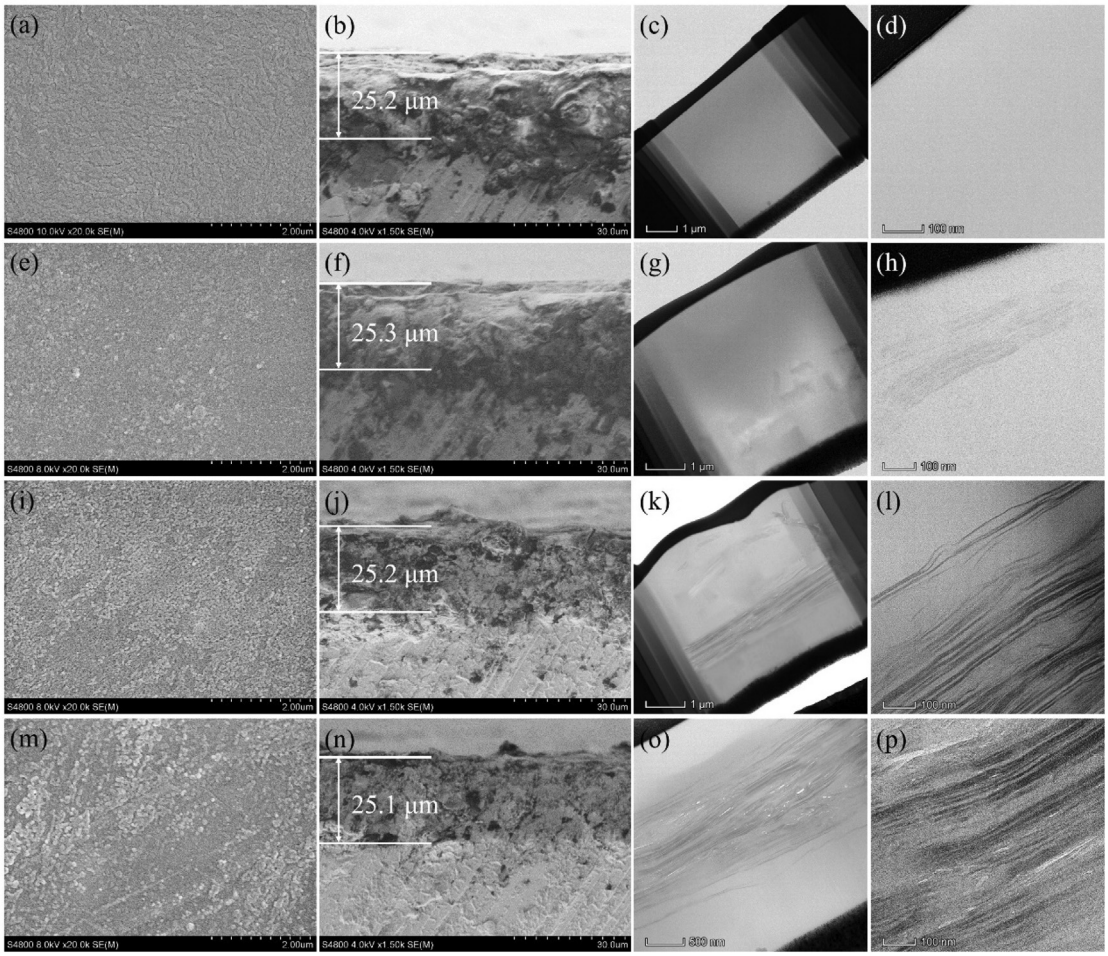

Fig. 4. Surface SEM, cross-sectional SEM, TEM and HRTEM images of (a–d) pure-EP, (e–h) 0.25%-DRGO$^+$/EP, (i–l) 0.5%-DRGO$^+$/EP, and (m–p) 1.0%-DRGO$^+$/EP coatings, respectively.

temperature increase rate of curing temperature is also beneficial to improve the self-alignment of DRGO$^+$ nanosheets during the coating formation process. The self-aligned parallel arrangement of DRGO$^+$ is conducive to improving the impermeability of epoxy coating, which can effectively prevent H_2O, O_2 and Cl^- in the corrosive medium from penetrating into the substrate, thus vastly improving the corrosion resistance of the composite coating.

3.4. Anti-corrosion performance

In order to evaluate the corrosion resistance of the composite coatings, the coatings are immersed in a 3.5 wt% NaCl solution for different times to measure the EIS. The Bode, Bode-Phase, and Nyquist plots of pure-EP, 0.25%-DRGO$^+$/EP, 0.5%-DRGO$^+$/EP, and 1.0%-DRGO$^+$/EP coatings are shown in Fig. 5. In general, the impedance modulus ($|Z|_{0.01Hz}$) at f = 0.01 Hz in the Bode plot (Fig. 5a, d, g, and j) reflects the coating's ability to suppress the current between the cathode and anode regions. The greater the impedance modulus of the coating, the better the protection [37]. The $|Z|_{0.01Hz}$ values of different coatings at different immersion times are shown in Fig. 6(c). For the pure-EP coating, the initial low-frequency impedance modulus is 4.07×10^9 Ω cm^2, and after 35 days of immersion, it drops sharply to 9.1×10^7 Ω cm^2, which is reduced by two orders of magnitude. It indicates that the corrosive medium has penetrated into the coating substrate through the defect, resulting in a decrease in the corrosion resistance of the coating. The initial $|Z|_{0.01Hz}$ of the 0.25%-DRGO$^+$/EP coating is 5.25×10^9 Ω cm^2, and after 35 days of immersion, the $|Z|_{0.01Hz}$ is 4.07×10^8 Ω cm^2. The value of the impedance modulus is increased relative to the pure-EP coating and the rate of decline is slower. It indicates that the incorporation of DRGO$^+$ into the epoxy coating is beneficial to improve the impermeability of the composite coating, so that the penetration rate of the corrosive medium in the coating becomes slower, resulting in an increase in the corrosion resistance of the coating. Surprisingly, the initial $|Z|_{0.01Hz}$ of the 0.5%-DRGO$^+$/EP coating is 4.79×10^{10} Ω cm^2, which is still as high as 7.08×10^9 Ω cm^2 after 35 days of immersion. This is ascribed to the parallel arrangement of the self-aligned DRGO$^+$ nanosheet in the epoxy coating, greatly improving the ability of the composite coating to resist the penetration of corrosive media. Likewise, the initial $|Z|_{0.01Hz}$ of 1.0%-DRGO$^+$/EP coating is also as high as 2.19×10^{10} Ω cm^2, but decreased than that of 0.5%-DRGO$^+$/EP coating, which may be the pores presence between the high content of graphene in the 1.0%-DRGO$^+$/EP composite coating.

The change of phase angle in Bode-Phase plots can also reflect the anti-corrosion of coating. Among them, the time constants at low frequencies and high frequencies correspond to the corrosion response of the metal substrate and the capacitance characteristics of the coating, respectively. When corrosive ions contact the substrate and cause metal corrosion, two time constants are generated in the Bode-Phase plots. The Bode-Phase plots of coatings at different immersion times are shown in Fig. 5(b, e, h, and k). Obviously, the pure-EP coating showed two time constants when immersed for 28 days, indicating that the corrosive medium in the corrosive solution had reached the substrate. At 35 days, the corrosion rate of the coating is prominently accelerated. However, the coating doped with DRGO$^+$ nanosheets still only shows one time constant, showing that the corrosive medium is still some

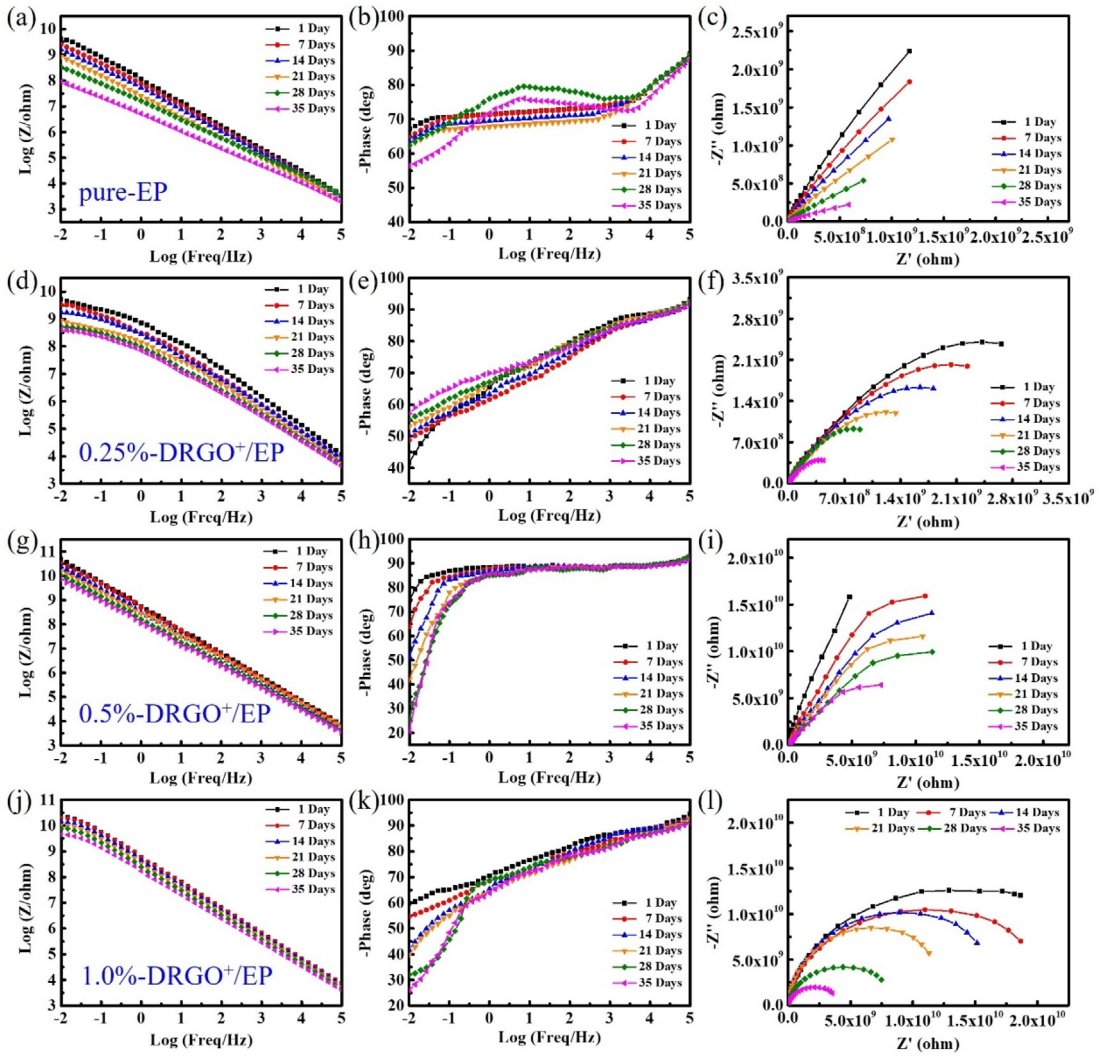

Fig. 5. Bode, Bode-Phase, and Nyquist plots of (a–c) pure-EP, (d–f) 0.25%-DRGO$^+$/EP, (g–i) 0.5%-DRGO$^+$/EP, and (j–l) 1.0%-DRGO$^+$/EP coatings in 3.5 wt% NaCl solution for different immersion times, respectively.

distance away from the interface between the coating and substrate. The above results indicate that the addition of DRGO$^+$ is beneficial to improving the barrier performance of the coating.

Fig. 5(c, f, i, and l) displays Nyquist plots of different samples at different immersion stages. Generally, it can be divided into two stages depending on whether the corrosive medium reaches the interface of the coating and the substrate, which corresponds to the time constant in the Bode-Phase plots discussed above. When the corrosive medium does not reach the substrate, its equivalent circuit model diagram is shown in Fig. 6(a), otherwise, as shown in Fig. 6(b) [38]. Where R_s is the resistance of the corrosion solution, R_c and Q_c correspond to the resistance and capacitance of the coating respectively, and R_{ct} and Q_{dl} represent the charge transfer resistance and double-layer capacitance [39]. The radius of the impedance arc in Nyquist plots can reflect the corrosion resistance of coating. The larger the radius, the better the corrosion resistance [40]. It can be seen that the corrosion resistance of all coatings decreases with the immersion time, but the 0.5%-DRGO$^+$/EP coating has the slowest rate of decline. In addition, the value of R_c decreases with the penetration of the corrosive medium, which can reflect the corrosion ease of the coating, the larger the value, the better the corrosion resistance of coating. The value of R_c obtained by fitting are shown in Fig. 6(d). After 35 days of immersion, the R_c of the pure-EP coating decreased from 4.84 × 10^9 to 6.3 × 10^8 Ω, especially when the corrosive medium penetrated the substrate (28 days), the R_c of the coating dropped sharply. However, the composite coating with DRGO$^+$ nanosheet has a slower resistance reduction, indicating a significant decrease in the penetration rate of the corrosive medium. After 35 days of immersion, the R_c of 0.5%-DRGO$^+$/EP coating is still up to 1.31 × 10^{10} Ω. The results show that the tight self-aligned parallel arrangement DRGO$^+$ can significantly improve the barrier performance of the composite coating. Similarly, the reason for the decrease in the R_c of the 1.0%-DRGO$^+$/EP coating is due to the presence of pores between the graphene in the coating. Therefore, adding appropriate content of DRGO$^+$ nanosheet in epoxy coating can observably improve the anti-corrosion of coating.

In order to verify the effect of the addition of DRGO$^+$ nanosheets on the barrier properties of the coating, the water absorption of the coating is calculated according to the Brasher and Kingsbury (BK) formula [41–43], as shown in Eq. (1) and Fig. 7.

$$X_v\% = \frac{\log \frac{C_c(t)}{C_c(0)}}{\log(80)} \times 100 \quad (1)$$

where X_v (%) represent the volume fraction of water in the coating, C_c (t) and C_c (0) represent the coating capacitance at time t and initial time, respectively. Obviously, the addition of DRGO$^+$ nanosheets can significantly reduce the water absorption of the coating. Furthermore, the 0.5%-DRGO$^+$/EP coating has the lowest water absorption,

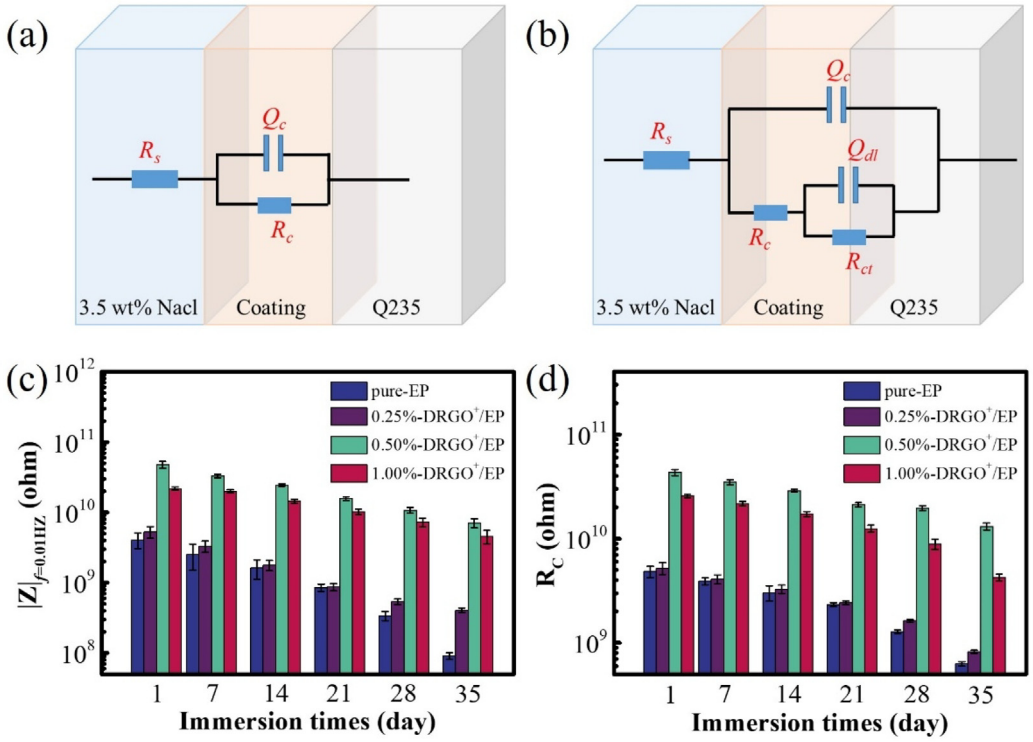

Fig. 6. Equivalent circuit model diagram of coatings at different stages (a, b); and $|Z|_{0.01Hz}$ (c) and R_c (d) of coatings at different immersion times.

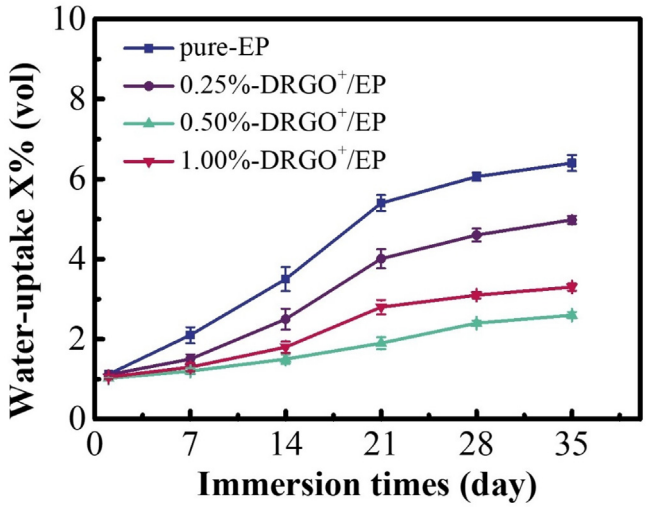

Fig. 7. Water absorption of coatings under different immersion times.

indicating that it has extraordinary barrier properties. This is determined by the closely self-aligned parallel arrangement of the RGO in the coating. The parallel arrangement of DRGO$^+$ nanosheets give full play to the interaction between graphene's high surface area and electrolyte, significantly improving the physical shielding of the coating and prolonging the penetration path of corrosive substances, thus greatly improving the corrosion resistance of the coating. Compared with other similar published works (Support Information Table S1), this study also shows better corrosion resistance.

Salt spray tests are employed to assess the anti-corrosion of industrial coatings. The optical images of pure-EP, 0.25%-DRGO$^+$/EP, 0.5%-DRGO$^+$/EP, and 1.0%-DRGO$^+$/EP coatings after salt spray experiments at 0, 240, and 480 h are shown in Fig. S3. It can be seen from the picture after the 240 h salt spray test that the pure-EP coating is covered with rust around the scratches, and a little rust spots appear in the undamaged area. The surface of the 0.25%-DRGO$^+$/EP coating has less rust than that of pure-EP coating. However, the surface of the 0.5%-DRGO$^+$/EP and 1.0%-DRGO$^+$/EP coatings remained intact except for rust around the scratch. After 480 h salt spray test, the pure-EP and 0.25%-DRGO$^+$/EP coatings are almost completely covered by rust, except that the 0.25%-DRGO$^+$/EP coating coverage area is less than that of the pure-EP coating. For the 0.5%-DRGO$^+$/EP coating, black spots appear around the scratches, but the surface remains intact. The 1.0%-DRGO$^+$/EP coating is covered by black spots around the scratch and has bright white spots on the surface. The results showed that the addition of DRGO$^+$ nanosheet is helpful to enhance the corrosion resistance of pure epoxy coating. When the content is 0.5 wt%, the composite coating has the best anti-corrosion owing to the tight parallel arrangement of DRGO$^+$ inside the coating.

In order to better determine the corrosion protection mechanism of the coatings, the LEIS test was performed by artificially introducing scratches on the surface of the coatings. The coating is immersed in 3.5 wt% NaCl solution for 24 h, and the admittance values of the area (3×3 mm^2) around the scratch are measured at 1 h, 12 h, and 24 h, respectively, as shown in Fig. 8. The admittance values in the figure can be divided into three areas: the complete coating, interface between the coating and the scratch and scratch. Clearly, the admittance distribution of different coatings near the scratch changes obviously with immersion time. With the increase of immersion times, pure-EP coating changed from light blue to yellow and then to deep red near the scratch, and the admittance value changed significantly, corresponding to the artificial scratch area expansion and depth increase, as shown in Fig. 8(a–c). For the 0.25%-DRGO$^+$/EP coating, the area around the scratch changed from light blue to green and then to red, the area and depth of the artificial scratch area are decreased compared with the pure-EP coating. It is indicated that the addition of DRGO$^+$ nanosheet is beneficial to enhance the corrosion resistance of epoxy coating. Surprisingly, the vicinity of the 0.5%-DRGO$^+$/EP coating scratches changed from light blue to light blue and then to green, the area and depth of the artificial scratched area are vastly reduced. This is ascribed to the tight self-aligned parallel arrangement of DRGO$^+$ in the

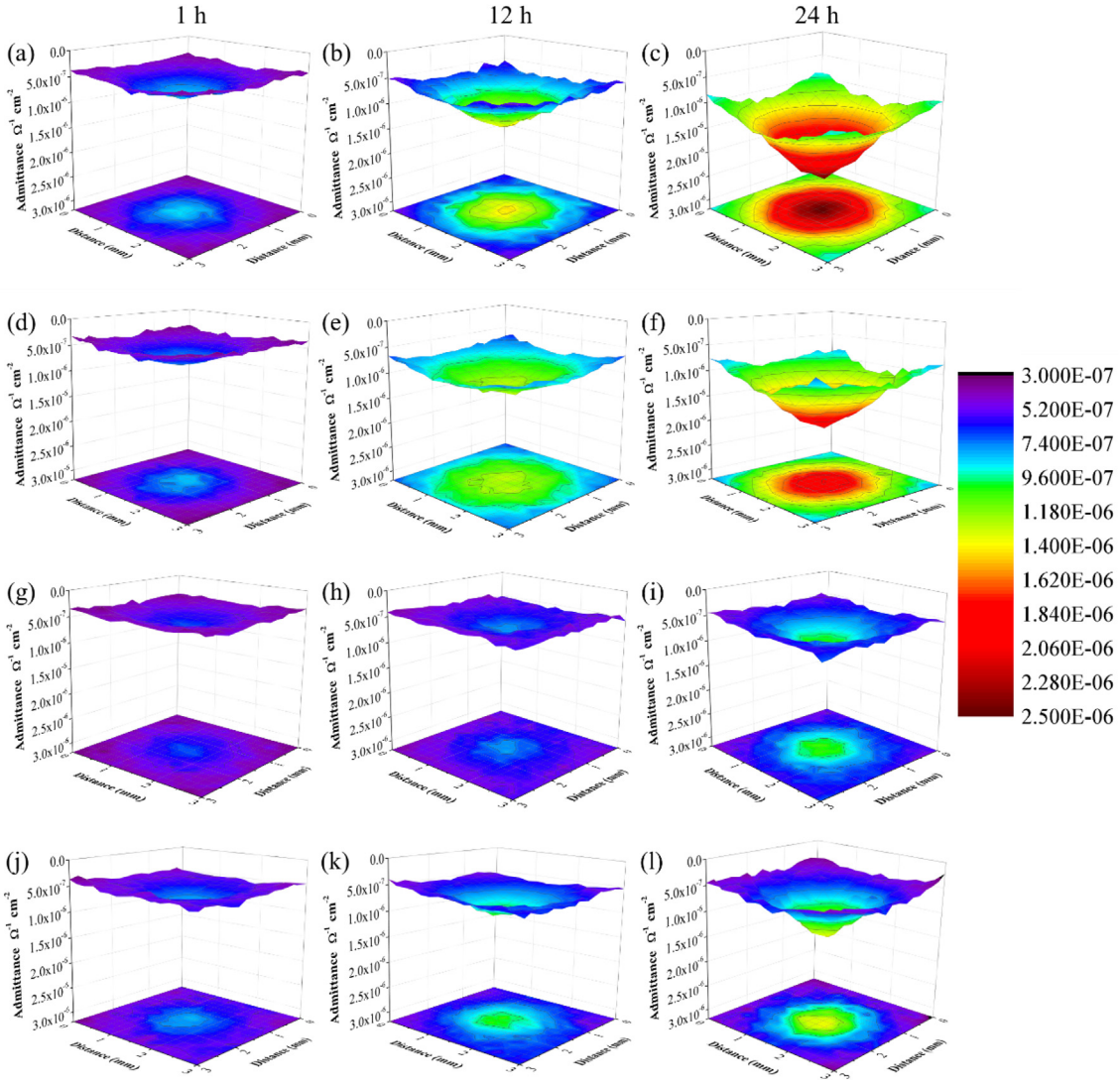

Fig. 8. LEIS maps of (a–c) pure-EP, (d–f) 0.25%-DRGO$^+$/EP, (g–i) 0.5%-DRGO$^+$/EP, and (j–l) 1.0%-DRGO$^+$/EP coatings at different immersion times.

composite coating, which immensely improves the barrier performance of the coating. For the 1.0%-DRGO$^+$/EP coating, the scratches changed from light blue to green and then to yellow. Compared with the pure-EP coating, the area and depth of the artificial scratch area are greatly reduced, but there is still different than that of the 0.5%-DRGO$^+$/EP coating. This is mainly because with the increase of DRGO$^+$ content in the coating, there will be small pores between the DRGO$^+$ in the coating, so that the corrosion resistance of the composite coating is reduced. This is consistent with the above EIS analysis.

3.5. Corrosion products analysis

In order to verify the corrosion protection effect of DRGO$^+$ nanosheet and reveal the protection mechanism of composite coatings, XRD and SEM were used to analyze the corrosion products of the coatings immersed in 3.5 wt% NaCl solution for 35 days. The coating on the surface of the Q235 carbon steel is removed and cleaned with ethanol before the corrosion products analysis. Fig. 9 reveals the XRD patterns of corrosion products on the surface of carbon steel under pure-EP, 0.25%-DRGO$^+$/EP, 0.5%-DRGO$^+$/EP, and 1.0%-DRGO$^+$/EP coatings. There are six distinct characteristic peaks in the XRD pattern of pure-EP coating, including Fe_3O_4 at 29.5°, FeOOH at 31.9°, α-Fe_2O_3 at 37.2°, and Fe at 44.7°, 65.0° and 82.2° [44–46]. It is indicated that the corrosion products under the pure-EP coating are mainly composed

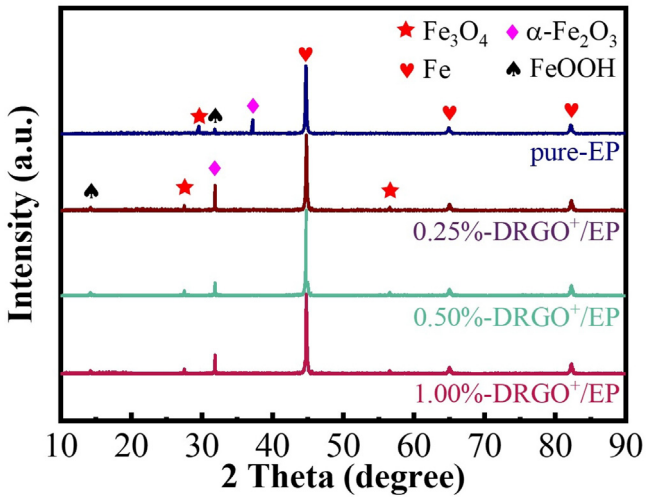

Fig. 9. XRD pattern of corrosion products on the surface of carbon steel under pure-EP, 0.25%-DRGO$^+$/EP, 0.5%-DRGO$^+$/EP, and 1.0%-DRGO$^+$/EP coatings.

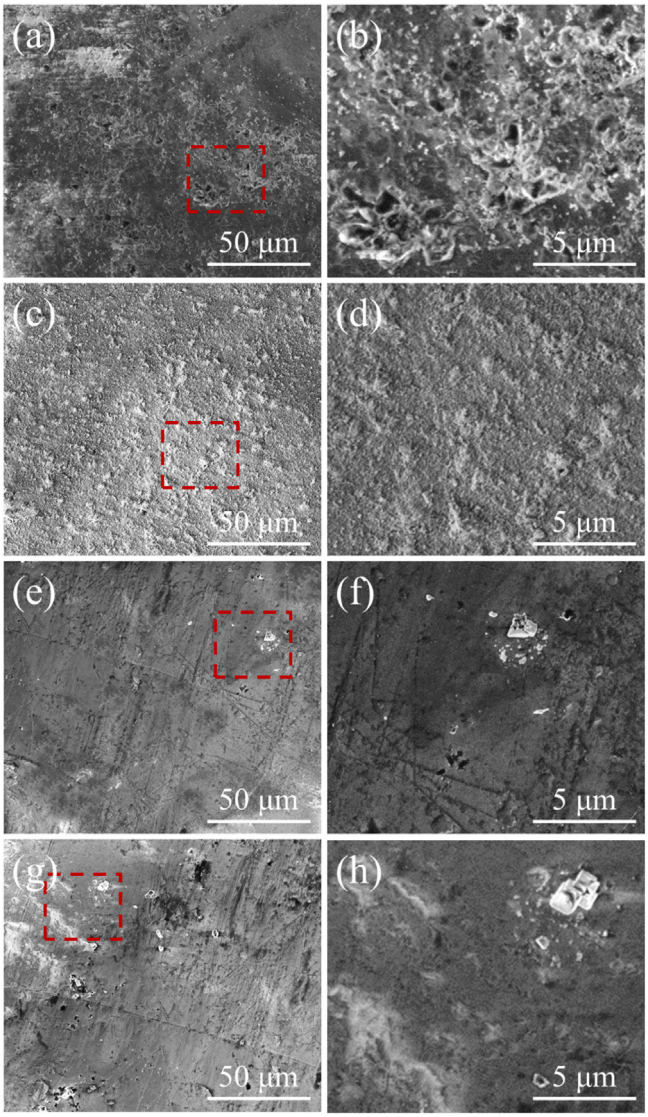

Fig. 10. SEM images of corrosion products on the surface of carbon steel under (a, b) pure-EP, (c, d) 0.25%-DRGO$^+$/EP, (e, f) 0.5%-DRGO$^+$/EP, and (g, h) 1.0%-DRGO$^+$/EP coatings.

of FeOOH and α-Fe_2O_3. In addition, the peak intensity of Fe in the pure-EP coating is lower than that of other composite coatings, which is mainly caused by the surface of the carbon steel under the pure-EP coating being covered by corrosion products. The corrosion products of 0.25%-DRGO$^+$/EP, 0.5%-DRGO$^+$/EP, and 1.0%-DRGO$^+$/EP composite coatings are mainly composed of Fe_3O_4 and Fe_2O_3 [47,48]. Moreover, the variation rule of corrosion product Fe_2O_3 content is consistent with the variation rule of corrosion resistance of coatings obtained by the above corrosion test analysis. The addition of DRGO$^+$ nanosheet is beneficial to improve the corrosion resistance of the coating, but when the content of DRGO$^+$ is greater than 0.5 wt%, the corrosion resistance of the composite coating will decrease.

The SEM images of the corrosion products on the surface of carbon steel under pure-EP, 0.25%-DRGO$^+$/EP, 0.5%-DRGO$^+$/EP, and 1.0%-DRGO$^+$/EP coatings are shown in Fig. 10. The surface of the pure-EP coating is severely corroded, causing corrosion pits and covering a thick layer of corrosion products. For the 0.25%-DRGO$^+$/EP coating, the corrosion pits on the surface and the covered corrosion products are much less than that of pure-EP coating, indicating that the addition of DRGO$^+$ nanosheet can effectively improve the corrosion resistance of the coating. However, the surface of the 0.5%-DRGO$^+$/EP coating has almost no corrosion products covering, except for a few etch pits. This is attributed to the presence of tight self-aligned parallel arrangement RGO in the coating, which can efficaciously blocks the penetration of corrosive media into the steel surface, thereby dramatically improving the corrosion resistance of the composite coating. For the 1.0%-DRGO$^+$/EP coating, although there are fewer corrosion pits and corrosion products on the surface, the corrosion resistance of the coating is lower than that of 0.5%-DRGO$^+$/EP coating. This is mainly because when the content of DRGO$^+$ nanosheet is high, holes will appear between RGO, which reduces the barrier and anti-corrosion of the coating.

3.6. Corrosion protection mechanism

The corrosion protection mechanism of pure-EP and 0.5%-DRGO$^+$/EP coatings are shown in Fig. 11. During the preparation of the coating and long-term immersion in the corrosive solution, defects are inevitably generated inside the coating. For the pure-EP coating (Fig. 11a), corrosive media such as H_2O, O_2, and Cl^- will penetrate into the substrate along the defects of the coating, forming microgalvanic corrosion in local areas, and the following reactions occur (Eqs. (2)–(4)). The formation of pitting pits on the metal surface further accelerates the corrosion and renders the coating ineffective.

$$Fe \rightarrow Fe^{2+} + 2e^- \quad (2)$$

$$H_2O + \frac{1}{2}O_2 + 2e^- \rightarrow 2OH^- \quad (3)$$

$$Fe^{2+} + 2OH^- \rightarrow FeOOH + H^+ + e^- \quad (4)$$

As for the 0.5%-DRGO$^+$/EP coating, the addition of DRGO$^+$ will fill in some defects in the coating or form a barrier network, which tremendously improves the physical barrier effect and anti-permeability of the composite coating. In addition, when the corrosive medium reaches the coating substrate, microgalvanic corrosion will also form in the local area (Eqs. (2)–(7)). However, the quaternary amino groups in DRGO$^+$ can generate electrostatic adsorption with electrons, which causes Fe^{2+} to be oxidized to Fe_2O_3 or Fe_3O_4, forming a dense passivation film on the surface of carbon steel.

$$Fe^{2+} \rightarrow Fe^{3+} + e^- \quad (5)$$

$$2Fe^{2+} + H_2O + O_2 + 2e^- \rightarrow Fe_2O_3 + 2H^+ \quad (6)$$

$$3Fe^{3+} + 2H_2O + O_2 + 5e^- \rightarrow Fe_3O_4 + 4H^+ \quad (7)$$

Importantly, the RGO itself used in this study is less conductive, and the $-NH_3^+$ in DRGO$^+$ can also absorb electrons generated during Fe oxidation, it does not accelerate the corrosion process of the coating. In addition, DRGO$^+$ has remarkable dispersion in water-based cathodic epoxy emulsion and can be self-aligned and parallel arranged in the coating under the action of electric field, so the uniform orientation of 0.5%-DRGO$^+$/EP coating further increases the tortuous path of the corrosive medium to the substrate. Moreover, the dense passivation film of carbon steel surface also can protect substrate from corrosion. Accordingly, the 0.5%-DRGO$^+$/EP coating exhibits extraordinary long-term anticorrosive performance.

4. Conclusions

In this study, the newfangled cationic dopamine-reduced graphene oxide (DRGO$^+$) nanosheets are successfully prepared as a fillers for epoxy coatings. Due to the presence of $-NH_3^+$, DRGO$^+$ can be stably dispersed in commercial water-based cathodic epoxy emulsion and can be tight self-aligned parallel arrangement in the composite coating under electric field. The EIS test showed that the initial low-frequency impedance modulus of the 0.5%-DRGO$^+$/EP coating is as high as 4.79×10^{10} Ω cm^2, which is an order of magnitude higher than that of the pure-EP coating (4.07×10^9 Ω cm^2). LEIS technology and corrosion product analysis revealed that the mechanism of anti-corrosion

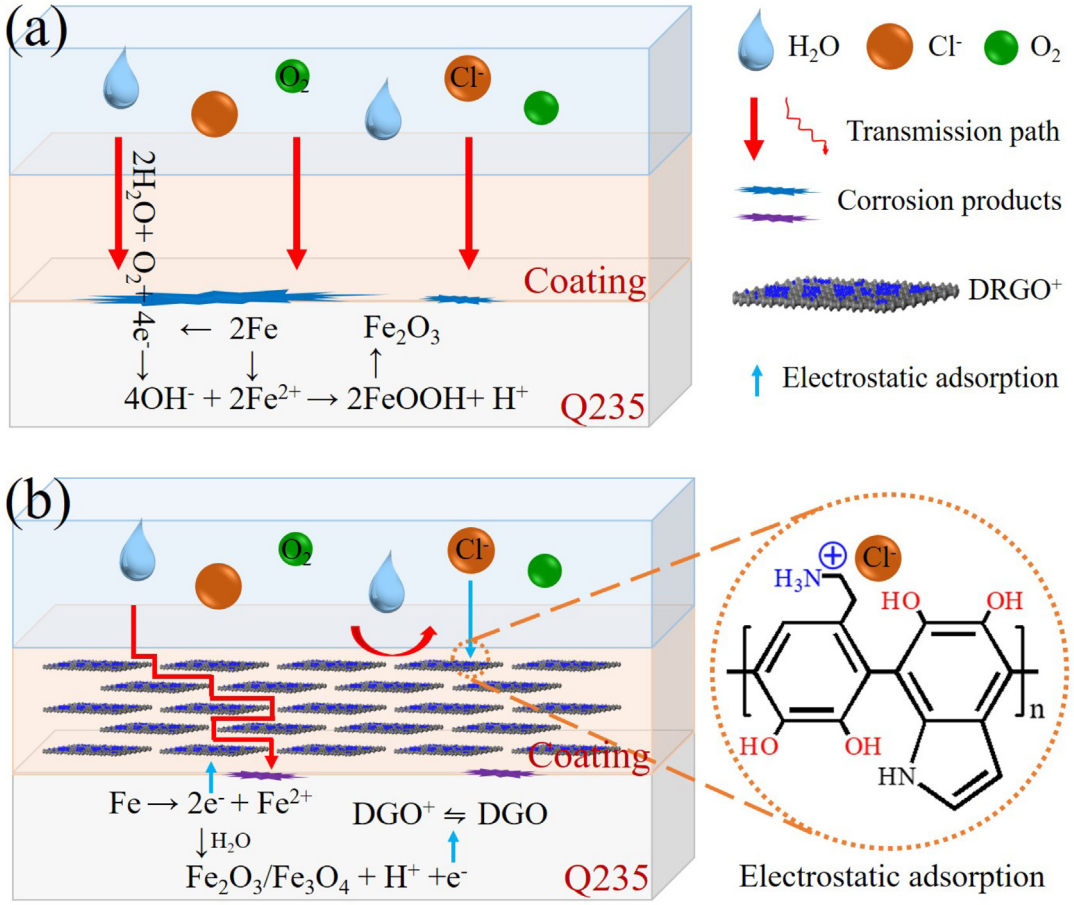

Fig. 11. Schematic images of corrosion protection mechanism of (a) pure-EP and (b) 0.5%-DRGO$^+$/EP coatings.

reinforcement of coating is: The addition of DRGO$^+$ can form a barrier network in the coating, which significantly improves the physical barrier effect of the coating and prolongs the penetration path of the corrosive medium, immensely improving the anti-corrosion of the coating. In addition, the positively charged –NH_3^+ on DRGO$^+$ can electrostatic attract electrons and corrosive negative ions, forming a dense oxide film (Fe_2O_3/Fe_3O_4) on the surface of the substrate. Therefore, this work provides a potential route to prepare coatings with extraordinary long-term corrosion resistance on a large scale.

Declaration of Competing Interest

The authors declare that they have no known competing financial interests or personal relationships that could have appeared to influence the work reported in this paper.

Acknowledgements

This work was supported by “The National Science Fund for Distinguished Young Scholars of China” (No. 51825505), Zhejiang Key Research and Development Program (2019C03093), Strategic Priority Research Program of the Chinese Academy of Sciences (No. XDA13040601) and “One Hundred Talented People” of the Chinese Academy of Sciences (No. Y60707WR04).

Appendix A. Supplementary data

The optical photos of different contents of DRGO$^+$ dispersed in epoxy emulsion. The zeta potential of the GO and DRGO$^+$ dispersed in deionized water (0.5 mg/mL). The optical images of (a) pure-EP, (b) 0.25%-DrGO$^+$/EP, (c) 0.5%-DrGO$^+$/EP, and (d) 1.0%-DrGO$^+$/EP coatings after salt spray experiments at 0, 240, and 480 h. Supplementary data to this article can be found online at https://doi.org/10.1016/j.cej.2020.124435.

References

[1] Y.J. Qiang, S.T. Zhang, B.C. Tan, S.J. Chen, Evaluation of Ginkgo leaf extract as an eco-friendly corrosion inhibitor of X70 steel in HCl solution, Corros. Sci. 133 (2018) 6–16.
[2] X.H. Luo, J.W. Zhong, Q.L. Zhou, S. Du, S. Yuan, Y.L. Liu, Cationic reduced graphene oxide as self-aligned nanofiller in the epoxy nanocomposited coating with excellent anticorrosive performance and its high antibacterial activity, ACS Appl. Mater. Interfaces 10 (2018) 18400–18415.
[3] L.M. Calado, M.G. Taryba, M.J. Carmezim, M.F. Montemor, Self-healing ceria-modified coating for corrosion protection of AZ31 magnesium alloy, Corros. Sci. 142 (2018) 12–21.
[4] J.H. Ding, H.R. Zhao, D. Ji, B.Y. Xu, X.P. Zhao, Z. Wang, D.L. Wang, Q.B. Zhou, H.B. Yu, Achieving long-term anticorrosion via the inhibition of graphene's electrical activity, J. Mater. Chem. A 7 (2019) 2864–2874.
[5] Y.J. He, I. Dobryden, J.S. Pan, A. Ahniyaz, T. Deltin, R.W. Corkery, P.M. Claesson, Nano-scale mechanical and wear properties of a waterborne hydroxyacrylic-melamine anti-corrosion coating, Appl. Surf. Sci. 457 (2018) 548–558.
[6] Z.X. Yu, H.H. Di, M. Yu, L. Liang, P. Yang, C.L. Zhang, H. Yi, Fabrication of graphene oxide–alumina hybrids to reinforce the anti-corrosion performance of composite epoxy coatings, Appl. Surf. Sci. 351 (2015) 986–996.
[7] S.H. Qiu, W. Li, W.R. Zheng, H.T. Zhao, L.P. Wang, Synergistic effect of polypyrrole-intercalated graphene for enhanced corrosion protection of aqueous coating in 3.5% NaCl solution, ACS Appl. Mater. Interfaces 9 (2017) 34294–34304.
[8] C.B. Liu, H.C. Zhao, P.M. Hou, B. Qian, L.P. Wang, An efficient graphene/cyclodextrin based nanocontainer: synthesis and host-guest inclusion for self-healing anticorrosion application, ACS Appl. Mater. Interfaces 10 (2018) 36229–36239.
[9] Y.W. Ye, Z.Y. Liu, L. Wei, D.W. Zhang, H.C. Zhao, L.P. Wang, X.G. Li, Superhydrophobic oligoaniline-containing electroactive silica coating as pre-process coating for corrosion protection of carbon steel, Chem. Eng. J. 348 (2018) 940–951.
[10] O. Yilmaz, A hybrid polyacrylate/OMMT nanocomposite latex: synthesis,

characterization and its application as a coating binder, Prog. Org. Coat. 77 (2014) 110–117.
[11] S. Wen, L.D. Wang, T.T. Wu, W. Meng, Z.Q. Yang, Y.Q. Pan, G.C. Liu, Inhibiting the corrosion-promotion activity of graphene, Chem. Mater. 27 (2015) 2367–2373.
[12] M.L. Mao, L. Jiang, L.C. Wu, M. Zhang, T.H. Wang, The structure control of ZnS/graphene composites and their excellent properties for lithium-ion batteries, J. Mater. Chem. A 3 (2015) 13384–13389.
[13] Y.Y. Li, Z.Z. Yang, H.X. Qiu, Y.G. Dai, J.H. Yang, Self-aligned graphene as anticorrosive barrier in waterborne polyurethane composite coatings, J. Mater. Chem. A 2 (2014) 14139–14145.
[14] Y.N. Singhbabu, B. Sivakumar, J.K. Singh, H. Bapari, A.K. Pramanick, R.K. Sahu, Efficient anti-corrosive coating of cold-rolled steel in a seawater environment using an oil-based graphene oxide ink, Nanoscale 7 (2015) 8035–8047.
[15] J.H. Ding, H.R. Zhao, X.P. Zhao, B.Y. Xu, H.B. Yu, How semiconductor transition metal dichalcogenides replaced graphene for enhancing anticorrosion, J. Mater. Chem. A 7 (2019) 13511–13521.
[16] C.H. Chang, T.C. Huang, C.W. Peng, T.C. Yeh, H.I. Lu, W.I. Hung, C.J. Weng, T.I. Yang, J.M. Yeh, Novel anticorrosion coatings prepared from polyaniline/graphene composites, Carbon 50 (2012) 5044–5051.
[17] Y. Su, V.G. Kravets, S.L. Wong, J. Waters, A.K. Geim, R.R. Nair, Impermeable barrier films and protective coatings based on reduced graphene oxide, Nat. Commun. 5 (2014) 4843.
[18] Y. Cui, S.I. Kundalwal, S. Kumar, Gas barrier performance of graphene/polymer nanocomposites, Carbon 98 (2016) 313–333.
[19] M.J. Cui, S.M. Ren, C. Jia, S. Liu, G.A. Zhang, H.C. Zhao, L.P. Wang, Q.J. Xue, Anticorrosive performance of waterborne epoxy coatings containing water-dispersible hexagonal boron nitride (h-BN) nanosheets, Appl. Surf. Sci. 397 (2016) 77–86.
[20] K.S. Triantafyllidis, P.C. Lebaron, I. Park, T.J. Pinnavaia, Epoxy–clay fabric film composites with unprecedented oxygen-barrier properties, Chem. Mater. 18 (2006) 4393–4398.
[21] E. Husain, T.N. Narayanan, J.J. Taha-Tijerina, S. Vinod, R. Vajtai, P.M. Ajayan, Marine corrosion protective coatings of hexagonal boron nitride thin films on stainless steel, ACS Appl. Mater. Interfaces 5 (2013) 4129–4135.
[22] O.C. Compton, S.B.T. Nguyen, Graphene oxide, highly reduced graphene oxide, and graphene: versatile building blocks for carbon-based materials, Small 6 (2010) 711–723.
[23] Y.W. Zhu, S. Murali, W.W. Cai, X.S. Li, J.W. Suk, J.R. Potts, R.S. Ruoff, Graphene and graphene oxide: synthesis, properties, and applications, J. Cheminformatics 22 (2010) 3906–3924.
[24] W. Lee, J.U. Lee, B.M. Jung, J.H. Byun, J.W. Yi, S.B. Lee, B.S. Kim, Simultaneous enhancement of mechanical, electrical and thermal properties of graphene oxide paper by embedding dopamine, Carbon 65 (2013) 296–304.
[25] H. Lu, S.T. Zhang, W.H. Li, Y.N. Cui, T. Yang, Synthesis of graphene oxide-based sulfonated oligoanilines coatings for synergistically enhanced corrosion protection in 3.5% NaCl solution, ACS Appl. Mater. Interfaces 9 (2017) 4034–4043.
[26] B. Ramezanzadeh, S. Niroumandrad, A. Ahmadi, M. Mahdavian, M.H.M. Moghadam, Enhancement of barrier and corrosion protection performance of an epoxy coating through wet transfer of amino functionalized graphene oxide, Corros. Sci. 103 (2016) 283–304.
[27] C.S. Lu, Y.W. Mai, Influence of aspect ratio on barrier properties of polymer-clay nanocomposites, Phys. Rev. Lett. 95 (2005) 088303.
[28] S.M. Kang, S. Park, D. Kim, S.Y. Park, R.S. Ruoff, H. Lee, Simultaneous reduction and surface functionalization of graphene oxide by mussel-inspired chemistry, Adv. Funct. Mater. 21 (2011) 108–112.
[29] I. Kaminska, M.R. Das, Y. Coffinier, J. Niedziolka-Jonsson, J. Sobczak, P. Woisel, J. Lyskawa, M. Opallo, R. Boukherroub, S. Szunerits, Reduction and functionalization of graphene oxide sheets using biomimetic dopamine derivatives in one step, ACS Appl. Mater. Interfaces 4 (2013) 1016–1020.
[30] Y.Q. Zhan, X.Y. Wan, S.J. He, Q.B. Yang, Y. He, Design of durable and efficient poly (arylene ether nitrile)/bioinspired polydopamine coated graphene oxide nanofibrous composite membrane for anionic dyes separation, Chem. Eng. J. 333 (2018) 132–145.
[31] C.Y. Wang, Y.F. Lan, W.T. Yu, L. Xing, Q. Yong, H.S. Liu, Preparation of amino-functionalized graphene oxide/polyimide composite films with improved mechanical, thermal and hydrophobic properties, Appl. Surf. Sci. 362 (2016) 11–19.
[32] A.K. Das, M. Srivastav, R.K. Layek, M.E. Uddin, D. Jung, N.H. Kim, J.H. Lee, Iodide-mediated room temperature reduction of graphene oxide: a rapid chemical route for the synthesis of a bifunctional electrocatalyst, J. Mater. Chem. A 2 (2014) 2055–2060.
[33] X.B. Zhu, X. Jiang, X.Y. Yao, Y.X. Leng, L.P. Wang, Q.J. Xue, Effective strategy for enhancing the performance of $Li_4Ti_5O_{12}$ anodes in lithium-ion batteries: magnetron sputtering molybdenum disulfide-optimized interface architecture, ACS Appl. Mater. Interfaces 11 (2019) 26880–26890.
[34] S. Stankovich, D.A. Dikin, R.D. Piner, K.A. Kohlhaas, A. Kleinhammes, Y. Jia, W. Yue, S.B.T. Nguyen, R.S. Ruoff, Synthesis of graphene-based nanosheets via chemical reduction of exfoliated graphite oxide, Carbon 45 (2007) 1558–1565.
[35] Z. Wang, Y. Dong, H. Li, Z. Zhao, H.B. Wu, C. Hao, S. Liu, J. Qiu, X.W. Lou, Enhancing lithium-sulphur battery performance by strongly binding the discharge products on amino-functionalized reduced graphene oxide, Nat. Commun. 5 (2013) 5002.
[36] Y. Dan, S. Huang, M.N. Ruan, S.X. Li, J.W. Yang, Y.B. Wu, W.L. Guo, L.Q. Zhang, Mussel inspired modification for aluminum oxide/silicone elastomer composites with largely improved thermal conductivity and low dielectric constant, Ind. Eng. Chem. Res. 57 (2018) 3255–3262.
[37] S.G. Zhou, X.B. Zhu, L.Q. Ma, Q.Q. Yan, S.C. Wang, Outstanding super-hydrophobicity and corrosion resistance on carbon-based film surfaces coupled with multi-walled carbon nanotubes and nickel nano-particles, Surf. Sci. 677 (2018) 193–202.
[38] E. Cano, D. Lafuente, D.M. Bastidas, Use of EIS for the evaluation of the protective properties of coatings for metallic cultural heritage: a review, J. Solid State Electr. 14 (2010) 381–391.
[39] J.B. Jorcin, M.E. Orazem, N. Pébère, B. Tribollet, CPE analysis by local electrochemical impedance spectroscopy, Electrochim. Acta 51 (2006) 1473–1479.
[40] S.G. Zhou, X.B. Zhu, Q.Q. Yan, S.C. Wang, Corrosion resistance and self-cleaning behaviour of Ni/a-C: H superhydrophobic films, Surf. Eng. 34 (2018) 611–619.
[41] V.N. Nguyen, F.X. Perrin, J.L. Vernet, Water permeability of organic/inorganic hybrid coatings prepared by sol–gel method: a comparison between gravimetric and capacitance measurements and evaluation of non-Fickian sorption models, Corros. Sci. 47 (2005) 397–412.
[42] A.-S.M. Del, L.M. Cárcel, I. Nevares, Characterization of the oxygen transmission rate of oak wood species used in cooperage, J. Agr. Food Chem. 65 (2017) 648–655.
[43] D.M. Brasher, A.H. Kingsbury, Electrical measurements in the study of immersed paint coatings on metal. I. Comparison between capacitance and gravimetric methods of estimating water uptake, J. Chem. Technol. Biot. 4 (2010) 62–72.
[44] J. Alcántara, B. Chico, I. Díaz, D.D.L. Fuente, M. Morcillo, Airborne chloride deposit and its effect on marine atmospheric corrosion of mild steel, Corros. Sci. 97 (2015) 74–88.
[45] Y.W. Ye, D.W. Zhang, Z.Y. Liu, L. Wei, H.C. Zhao, L.P. Wang, X.G. Li, Anti-corrosion properties of oligoaniline modified silica hybrid coatings for low-carbon steel, Synthetic Met. 235 (2018) 61–70.
[46] M.J. Cui, S.M. Ren, S.L. Qin, Q.J. Xue, H.C. Zhao, L.P. Wang, Processable poly(2-butylaniline)/hexagonal boron nitride nanohybrids for synergetic anticorrosive reinforcement of epoxy coating, Corros. Sci. 131 (2018) 187–198.
[47] T. Ohtsuka, S. Tanaka, Monitoring the development of rust layers on weathering steel using in situ Raman spectroscopy under wet-and-dry cyclic conditions, J. Solid State Electr. 19 (2015) 3559–3566.
[48] Y.W. Ye, D.W. Zhang, T. Liu, Z.Y. Liu, W. Liu, J.B. Pu, H. Chen, H.C. Zhao, X.G. Li, Improvement of anticorrosion ability of epoxy matrix in simulate marine environment by filled with superhydrophobic POSS-GO nanosheets, J. Hazard. Mater. 364 (2019) 244–255.